Transforming a strain-stabilized ferroelectric into an intrinsic polar metal with light

Alon Ron,[1] Kaveh Ahadi,[2] Daniel Hickox-Young,[3] Danilo Puggioni,[3] Omar Mehio,[4,5] James M. Rondinelli,[3] Susanne Stemmer,[2] and David Hsieh[4,5]

[1]*Raymond and Beverly Sackler School of Physics and Astronomy, Tel-Aviv University, Tel Aviv 69978, Israel*
[2]*Materials Department, University of California, Santa Barbara, California 93106, USA*
[3]*Department of Materials Science and Engineering, Northwestern University, Evanston, Illinois 60208, USA*
[4]*Department of Physics, California Institute of Technology, Pasadena, California 91125, USA*
[5]*Institute for Quantum Information and Matter, California Institute of Technology, Pasadena, California 91125, USA*

(Received 22 April 2022; revised 4 September 2023; accepted 28 November 2023; published 22 December 2023)

We explore the effects of chemical doping and photodoping in the strain-induced multiferroic $EuTiO_3$ grown on $DyScO_3$ substrates. The polar order is probed experimentally using second harmonic generation (SHG) and modeled using *ab initio* calculations. At low photodoping concentrations, we observe a reduction in SHG signal, indicating a destructive coupling between charge carriers and polar order in accordance with our simulations and expectations for a second-order Jahn-Teller driven ferroelectric. However, under increased photodoping the reduction in SHG plateaus at 84% of its original magnitude, indicating resilience of the polar order in the presence of a high concentration of delocalized electrons. This behavior stands in contrast with our first-principles simulations, indicating that $EuTiO_3$ undergoes a transition from ferroelectric to polar metallic character under photodoping. We suggest several hypotheses for the mechanism behind this change in distortion character.

DOI: 10.1103/PhysRevB.108.224308

I. INTRODUCTION

Metallicity and long-range polar order were long thought to be fundamentally incompatible, due to the screening of electric dipoles by free charges. However, their possible coexistence was suggested in 1965 [1] and recently validated by the synthesis of the first polar metal, $LiOsO_3$ [2]. Rondinelli and Puggioni subsequently designed and successfully implemented an operational principle termed the "weak-coupling hypothesis" [3], namely that in order for metallic conductivity to coexist with coordinated polar displacements the two orders must be decoupled from one another. Consequently, when charge carriers are introduced to otherwise insulating or semiconducting polar systems (i.e., doped ferroelectrics) the resulting compounds may be classified according to the response of the polar instability to the change in conductivity. On the one hand, the response may be the destruction of the polar order, as observed in second-order Jahn-Teller (SOJT)-driven proper ferroelectrics such as $BaTiO_3$ [4,5]. These materials may exhibit regimes that combine modest conductivity without inversion symmetry, but the two orders are still fundamentally contraindicated. On the other hand, the structural instability may persist unperturbed in response to additional free charge carriers, indicating a fundamentally compatible relationship similar to that observed in polar metals [2,4,6].

Unstrained $EuTiO_3$ is an antiferromagnetic (AFM) paraelectric (PE) insulator. Epitaxial strain can drive $EuTiO_3$ into a SOJT-driven polar phase exhibiting both ferroelectric (FE) and ferromagnetic (FM) character [7,8]. In particular, experiments show that the application of a tensile epitaxial strain greater than 1% drives $EuTiO_3$ into a multiferroic FE-FM insulator with transition temperatures of ∼250 K (FE) and ∼4.2 K (FM) [8].

Both transitions—from AFM to FM and from PE to FE—are correlated with the position of the Ti ion inside its octahedral O_6 cage. Unstrained, $EuTiO_3$ has a cubic $Pm\bar{3}m$ structure and the undistorted cage provides a single well potential for Ti with its minimum at the center of the cage. When tensile epitaxial strain is applied, the lower-symmetry and elongated in-plane lattice parameters transform the single well potential into a double well. The Ti ion seeks to optimize its local bonding environment and displaces away from the center of the unit cell into either of the two degenerate minima, providing the conditions for a FE phase with $mm2$ point symmetry [8].

The strain-induced polar phase of $EuTiO_3$ is an attractive candidate for exploring the intersection of metallic conductivity and broken inversion symmetry. Although, as a SOJT-driven FE, we would expect additional charge carriers to disrupt the polar order, $EuTiO_3$ may be distinguished from prototypical SOJT-driven ferroelectrics by the presence of Eu f states which both form the valence band and lead to FM ordering. Additionally, and in contrast with conventional ferroelectrics [9], we observe that Eu strongly contributes to the low-lying transverse optical modes in $EuTiO_3$ [Figs. 1(a) and 1(b)] likely due to the close proximity of the f electron valence band and the Fermi energy.

In this Letter, we probe the interplay between doping and the polar order of strain-induced multiferroic $EuTiO_3$ experimentally computationally. We find that the strained samples exhibit an initial reduction in their polar distortion amplitude under low levels of chemical doping and photodoping, consistent with predictions from density functional calculations

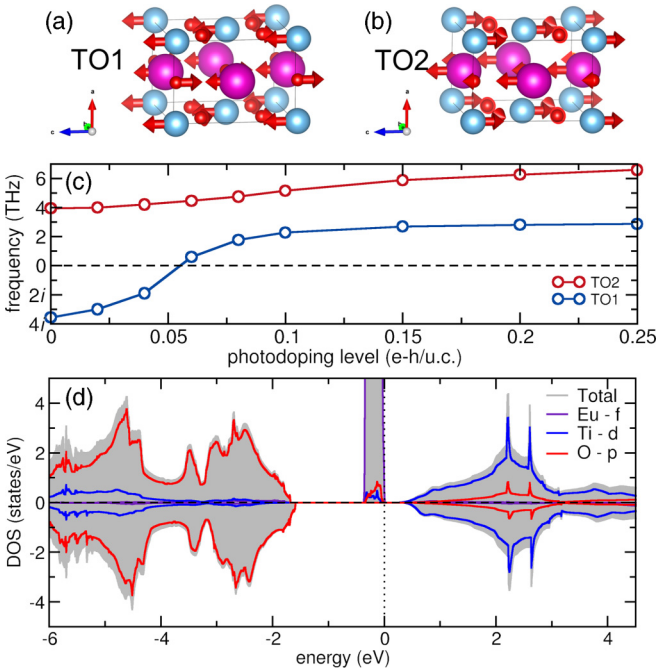

FIG. 1. (a), (b) TO1 and TO2 mode eigendisplacements at Γ for $EuTiO_3$ on $DyScO_3$. Large purple atoms depict Eu, small red atoms depict O, and midsize blue atoms depict Ti. Arrow lengths indicate relative displacement amplitudes. (c) Evolution of the Γ-centered TO1 and TO2 phonon modes for centrosymmetric tetragonal $P4/mmm$ $EuTiO_3$ upon increasing the photodoped-carrier concentration at 1.5% strain relative to the relaxed structure. (d) Spin-resolved electronic density of states (DOS) for ferromagnetic $P4/mmm$ $EuTiO_3$ at 1.5% strain, where the positive and negative y axes refer to majority and minority spin states, respectively.

(DFT) and in line with expectations for a SOJT-driven FE. At higher levels of doping, however, we find that the polar amplitude saturates at ∼84% of its original magnitude, indicating that the structural distortion is decoupled from the Fermi level. We offer several hypotheses to explain this change in character, ranging from nanostructural origins to a possible change in the driving mechanism of the displacive distortion.

II. DENSITY FUNCTIONAL THEORY RESULTS

To investigate the competing influences of strain and doping, we use DFT calculations [10]. We compute the in-plane tensile strain dependence of the Γ-point phonon modes while relaxing the out-of-plane lattice parameter. The model structure initially exhibits cubic ($Pm\bar{3}m$) symmetry, but immediately adopts $P4/mmm$ symmetry as tetragonality is enforced by the in-plane strain. Consistent with previous experimental and theoretical work [7,11], a polar instability arises as indicated by softening of the transverse optical TO1 mode at the Γ point (Fig. S1 in Supplemental Material [10]). The resulting twofold degenerate polar mode exhibits predominantly Slater character [12], which is enhanced by strain (Fig. S2 in Supplemental Material [10]). To investigate whether strain modulates the mixing between modes of different character—namely the TO1 (Slater) and TO2 (Last) modes (see Ref. [9] for canonical perovskite displacement patterns)—we also plotted the evolution of the TO2 mode. However, the strain-dependent dispersion of the TO2 mode is largely decoupled from changes in the TO1 mode.

We next examine the evolution of the polar distortion under photodoping [10] at 1.5% tensile strain (3.946 Å) relative to the relaxed structure, which is within the FE region of the previously calculated strain phase diagram [7,11]. The soft TO1 mode initially persists under photodoping before quickly stabilizing at a dopant concentration of approximately 0.06 electrons per unit cell (e/u.c.) or $\approx 10^{21}$ cm^{-3} [Fig. 1(c)]. This stabilization of the high-symmetry phase matches our expectation of doped, SOJT-driven d^0 FEs. The nonzero occupancy of the Ti d orbitals, which form the conduction band [Fig. 1(d)], disrupts the Ti-O covalent bonding driving local off-centering via the SOJT effect [5,13]. As with our observations under strain, whereas the TO1 mode undergoes significant changes, the TO2 mode is relatively unperturbed. This is consistent with their displacement patterns, since the TO1 (Slater) mode is dominated by Ti displacing relative to the oxygen octahedron while in the TO2 (Last) mode, Ti and O displace in the same direction and therefore are not driven by Ti-O bonding [9]. Similar calculations with electron doping (i.e., occupation of Ti 3d states) alone led to a nearly identical critical concentration (Fig. S3 of Supplemental Material [10]), indicating electrons in the conduction band are responsible for impeding the polar distortion (as opposed to the holes in the valence band), again in line with expectations for a SOJT-driven FE.

III. THIN FILM GROWTH AND CHARACTERIZATION

To test our theoretical predictions, we studied the evolution of the FE order parameter using optical second harmonic generation (SHG) [14] in epitaxially strained $EuTiO_3$ thin films as a function of chemical doping and photodoping. Epitaxial, 20-nm-thick Sm-doped $EuTiO_3$ layers were grown by molecular beam epitaxy (MBE) on (110) $DyScO_3$ single-crystal substrates. Elemental europium and a metalorganic compound, titanium tetraisopropoxide (TTIP), were used to supply Eu, Ti, and oxygen. We did not supply oxygen as TTIP provides oxygen. This technique provides an adsorption control growth window with extremely high-quality films, which were described elsewhere [15]. An x-ray diffraction pattern given in the Supplemental Material [10] shows thickness fringes, indicating smooth films with high structural quality. Substitution of Eu with Sm was performed following Ref. [16]. The substitution results in a static electronic occupation of the Ti t_{2g} orbitals. In these previous studies, metallic $Eu_{1-x}Sm_xTiO_3$ films were deposited on $(LaAlO_3)_{0.3}(Sr_2TaAlO_6)_{0.7}$ (LSAT), where the epitaxial strain is compressive so the film was not in a FE state. Here, we grew $Eu_{1-x}Sm_xTiO_3$ 20-nm thin films with $x = 0$ (undoped) and $x = 0.015$ (doped) on $DyScO_3$ substrates. The metallic properties of the doped sample were characterized by resistivity and Hall effect measurements, using the van der Pauw configuration, in magnetic fields between −0.6 and 0.6 T (Fig. 2).

SHG measurements were performed by shining 1.5 eV photons from a 100-kHz Ti:sapphire amplifier at an angle of 10° relative to the sample normal with S or P polarization and a pulse duration of ∼100 fs. The reflected beam at 1.5 eV was

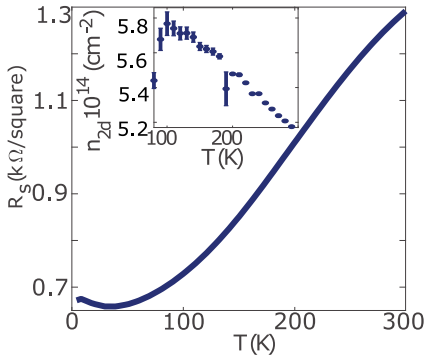

FIG. 2. Electrical characterization of the doped sample. Sheet resistance as a function of temperature. The behavior is metallic down to 4.2 K. A small upturn in resistivity at low temperatures is associated with strengthening of the FE order. Inset: Two-dimensional (2D) carrier density inferred from the slope of the Hall effect.

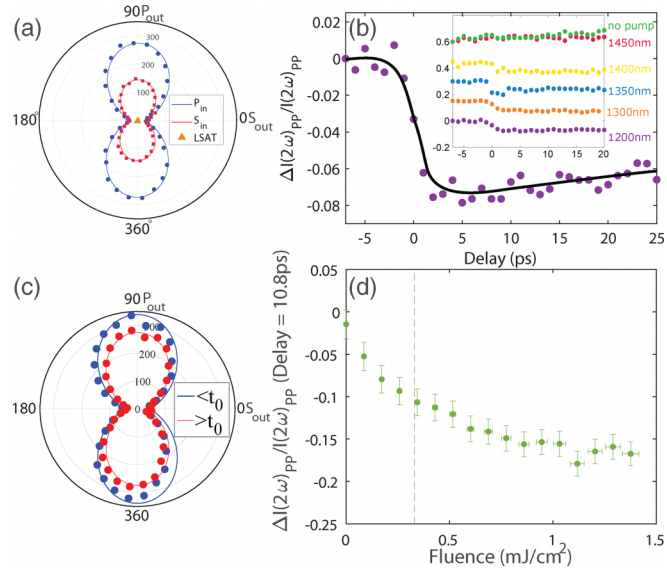

FIG. 3. (a) SHG intensity as a function of analyzer angle for the doped sample. Triangles near zero intensity are measurements on a nonpolar film grown on LSAT which is five orders of magnitude smaller. (b) SHG intensity as a function of time delay relative to the pump pulse for 1200 nm excitation. Other wavelengths are shown in the inset. (c) Polar plots in the P_{in} geometry as before and after (∼10 ps) the pump-pulse excitation at 1200 nm. (d) Fluence dependence of the SHG intensity ∼10 ps after the pump-pulse excitation at 1200 nm. The dashed line represents the fluence at which the photodoping equals the threshold for stabilization of the nonpolar phase found in our calculations (0.06 e/u.c.) assuming a quantum efficiency of 1. The vertical error bars are determined by the statistical noise of the camera. The fluence error bars are due to the lack of uniformity of the pump intensity throughout the thickness of the sample (see Supplemental Material Sec. V [10]).

filtered and the second harmonic at an energy of 3 eV was analyzed by rotating a linear polarizer. Transient SHG and reflectivity measurements were performed using the same probe beam (1.5 eV) and pumped with the signal beam of an optical parametric amplifier tunable between 1200 nm (∼1 eV) and 1450 nm (∼0.85 eV). Data were acquired at 80 K (below the FE transition of the strained undoped system [8]). Figure 3(a) shows the SHG intensity obtained from the doped film as a function of the analyzer angle. For both P and S polarization configurations a strong SHG signal in agreement with point group $mm2$ is observed, indicative of the polar nature of the film. This is consistent with our first-principles results, which indicate that this level of Sm doping ($x = 0.015$) should be well below the critical threshold for stabilizing the centrosymmetric structure ($x \sim 0.06$). For comparison, a similar measurement was performed on an unstrained film grown on an LSAT substrate from which the signal was five orders of magnitude weaker and shows the absence of polar order in agreement with Ref. [8].

IV. TIME-RESOLVED SHG RESULTS

To rapidly achieve a series of higher doping levels, we performed a time-resolved SHG-probe photodoping experiment on an undoped tensile strained $EuTiO_3$ sample grown on $DyScO_3$. The SHG signal was collected as a function of delay time relative to a pump-pulse excitation. The optical band gap of unstrained $EuTiO_3$ is ∼0.9 eV (1378 nm) [17]. As shown in Fig. 3(b), when the pump and probe pulses synchronously overlap on the sample surface (delay = 0) a drop in the SHG signal is observed only for photon energies which exceed this energy gap, indicating that the gap of the strained system is similar to that of the unstrained one. This drop is then followed by a slow relaxation time. Figure 3(c) shows SHG anisotropy plots before and after the pump excitation with 1 eV photon energy. The weakening of the SHG signal does not change the symmetry of the film and indicates that the FE order is weakened but not completely quenched. In an attempt to fully quench the FE order by photodoping, we increase the pump-pulse fluence well beyond the threshold predicted by DFT while keeping the photon energy constant to 1 eV, as shown in Fig. 3(d).

In contrast with the DFT results, we find the SHG signal saturates at the higher end of the fluence range. Saturation in optical experiments is expected when the pump excitation creates photobleaching, in our case filling (emptying) the Eu $4f$ (Ti $3d$) bands, corresponding to a sheet density of ∼4.5×10^{19} C/m^2. We test the photobleaching scenario by measuring the pump-probe reflectivity on undoped $EuTiO_3$ samples as a function of pump fluence with a pump photon energy of 1 eV. As shown in Fig. 4(a), a drop in the reflectivity of the probe beam is observed followed by a ∼100 fs recovery to a lower value than in equilibrium. Figure 4(b) shows the reflectivity dynamics as a function of pump fluence. The reflectivity response to the pump excitation grows monotonically with fluence, as can be seen by the increasing magnitude of the pump-probe signal and remains in the linear-response regime for fluences greater than those used in the SHG experiment [Fig. 4(b)]. As the same pump conditions were used for both the SHG and reflectivity experiments, we deduce that the origin for the saturation in the former is not photobleaching as it would have produced saturation in both experiments.

Reduction of the SHG signal could be caused by pump-induced heating. Since the measurements were performed

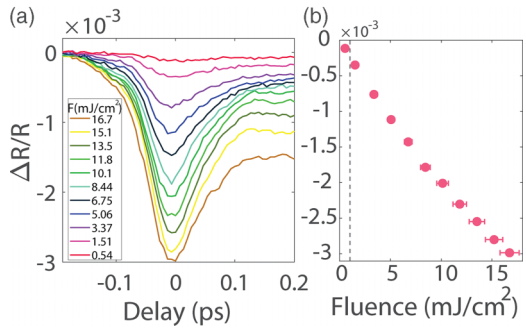

FIG. 4. (a) Linear pump-probe reflectivity as function of pump fluence with a wavelength of 1200 nm. (b) Reflectivity signal at the minima of the pump-probe traces shown in (a). The fluence error bars are due to the lack of uniformity of the pump intensity throughout the thickness of the sample (see Supplemental Material Sec. V [10]). The dashed line marks the saturation fluence value for SHG.

at 80 K, below the FE transition temperature (250 K), an increase in temperature will result in decreasing the signal. While consistent with our wavelength-dependent measurement [Fig. 3(a), inset] showing a decrease of the SHG signal only above the energy gap of $EuTiO_3$, it is inconsistent with our saturating fluence dependence. Furthermore, if heating caused the reduction of the FE order, saturation would have been expected only for complete quenching of the order (heating above the transition temperature) and not the observed finite $\sim -16\%$ reduction. Saturation to a nonzero value stems from a different mechanism, associated with the occupation of Ti t_{2g} states responsible for the SOJT effect driving the distortion.

The DFT prediction of high-symmetry stabilization under photodoping stands in stark contrast with the experimental evidence of persistent polar order ($\sim$84% of the undoped distortion magnitude) despite carrier concentrations well beyond the 10^{21} cm^{-3} threshold predicted by DFT. Surprisingly, $EuTiO_3$ on $DyScO_3$ appears to change character under photodoping. Initially, the material behaves as a doped SOJT-driven ferroelectric as new charge carriers reduce the magnitude of the polar distortion. Yet under increased photodoping, this reduction saturates to the point that the structural distortion appears fully decoupled from the Fermi level, a behavior associated with polar metals.

V. DISCUSSION

The discrepancy between simulation and experiment led to a reexamination of two assumptions inherent to the simulations, which may be unrealized in experiment: long-range cooperative displacements and a uniform distribution of free charge carriers. First, even low concentrations of charge carriers are sufficient to screen long-range Coulombic interactions in ferroelectrics [4].

In the absence of these interactions, the impetus for dipoles to align with one another decreases, allowing for the formation of nanodomains with different orientations of their polarization vector. Such nanodomains—on the order of several unit cells—have been observed to persist in isoelectronic and isostructural $SrTiO_3$ in the absence of long-range ordering [18]. However, despite inversion symmetry being locally broken in each domain, the SHG signals from different domains should destructively interfere because the optical wavelength far exceeds the domain size. Therefore, the nanodomain scenario alone cannot explain the discrepancy between theory and experiment.

For the second scenario, we suspect that doping may occur inhomogeneously within the film. This was observed in $BaTiO_3$ powders, where doping with oxygen vacancies led to the formation of two competing phases: one polar and insulating and the other centrosymmetric and metallic [19]. If a similarly inhomogeneous distribution of free charge occurred in $EuTiO_3$, the most highly doped regions would recover centrosymmetry as predicted in Fig. 1 while the less doped regions would persist and exhibit *mm*2 symmetry. This may seem unlikely since the inhomogeneity of photodoping under our experimental conditions is estimated to be $\sim$5.4% (see Supplemental Material Sec. V [10]). Domain structures have also been shown to redistribute free charge carriers in both $SrTiO_3$ and $BiFeO_3$ [20,21], where the electronic properties of domain walls differ substantially from the bulk. The nature of domain walls in strained $EuTiO_3$ is currently unknown but could be explored in order to identify a possible interaction with free charge carriers.

For the third and final scenario, we suggest that the persistent polar order in $EuTiO_3$ under photodoping may derive from coupling between the electronic and crystallographic structures. We observed an unusually large contribution from Eu in the $EuTiO_3$ TO1 mode [Fig. 1(a)] and previously noted that the presence of f states in the band structure distinguishes $EuTiO_3$ from other compounds. Depletion of the Eu f states via photodoping has previously been linked to structural changes [22], though to our knowledge this has not been investigated in the strained system. Our ability to investigate this avenue is limited by our photodoping approximation. Whereas we have attempted to reproduce direct excitation, constrained depletion of the valence band in proportion to conduction band electrons across the Brillouin zone fails to allow both electrons and holes to redistribute to their lowest-energy configuration. A more sophisticated photodoping method, which allows for independent electron and hole chemical potentials [23], is recommended for further investigation of photodoped $EuTiO_3$ deposited on $DyScO_3$.

These three scenarios are not mutually exclusive. On the contrary, it is probable that a combination of an inhomogeneous local structure (be it structural disorder and/or an uneven distribution of charge carriers) and an unusual *A*-site contribution to the soft phonon mode produces the observed experimental results. Further elucidation of the mechanism behind the surprising persistence of polar order in photodoped strained $EuTiO_3$ requires additional study. Pump-probe x-ray diffraction or *in situ* transmission electron microscopy concurrent with optical excitation would enable direct observation of the atomic positions that would clarify the local crystallographic structure, and more sophisticated photodoping simulations (as alluded to before) may identify more precisely the significance of the Eu f states forming the valence band.

VI. CONCLUSION

We reported a theoretical and experimental investigation of the evolution of the polar order in $EuTiO_3$ as a function of chemical doping and photodoping. We found at intermediate doping levels of 0.015 e/u.c. that a polar metallic state could be stabilized in equilibrium within similar doping levels of other oxide-based systems [24]. We further showed via SHG measurements that $EuTiO_3$ on $DyScO_3$ undergoes a change in character under photodoping, initially exhibiting a suppression of the polar order associated with doped SOJT-driven ferroelectrics before saturating at higher doping levels in contrast with what is predicted by first-principles calculations. We suggest several hypotheses for the origin of this transition to polar metal-like behavior and encourage further study of this metallic multiferroic.

ACKNOWLEDGMENTS

A.R. acknowledges support from the Zuckerman Foundation, and the Israel Science Foundation (Grant No. 1017/20). Sample growth, characterization, and optical spectroscopy measurements were supported by ARO MURI Grant No. W911NF-16-1-0361. J.M.R. and D.H.Y. were supported by the National Science Foundation (NSF) under Award No. DMR-1729303. S.S. and K.A. acknowledge support by the National Science Foundation (NSF) under Award No. DMR-1729489. D.P. was funded by the Army Research Office (ARO) under Grant No. W911NF-15-1-0017. Calculations were performed using the Department of Defense – High Performance Computing Modernization Program (DOD-HPCMP).

[1] P. W. Anderson and E. Blount, Symmetry considerations on martensitic transformations: "Ferroelectric" metals? Phys. Rev. Lett. **14**, 217 (1965).

[2] Y. Shi, Y. Guo, X. Wang, A. J. Princep, D. Khalyavin, P. Manuel, Y. Michiue, A. Sato, K. Tsuda, S. Yu *et al.*, A ferroelectric-like structural transition in a metal, Nat. Mater. **12**, 1024 (2013).

[3] D. Puggioni and J. M. Rondinelli, Designing a robustly metallic noncenstrosymmetric ruthenate oxide with large thermopower anisotropy, Nat. Commun. **5**, 3432 (2014).

[4] H. J. Zhao, A. Filippetti, C. Escorihuela-Sayalero, P. Delugas, E. Canadell, L. Bellaiche, V. Fiorentini, and J. Íñiguez, Metascreening and permanence of polar distortion in metallized ferroelectrics, Phys. Rev. B **97**, 054107 (2018).

[5] D. Hickox-Young, D. Puggioni, and J. M. Rondinelli, Persistent polar distortions from covalent interactions in doped $BaTiO_3$, Phys. Rev. B **102**, 014108 (2020).

[6] N. Laurita, A. Ron, J.-Y. Shan, D. Puggioni, N. Koocher, K. Yamaura, Y. Shi, J. Rondinelli, and D. Hsieh, Evidence for the weakly coupled electron mechanism in an Anderson-Blount polar metal, Nat. Commun. **10**, 3217 (2019).

[7] C. J. Fennie and K. M. Rabe, Magnetic and electric phase control in epitaxial $EuTiO_3$ from first principles, Phys. Rev. Lett. **97**, 267602 (2006).

[8] J. H. Lee, L. Fang, E. Vlahos, X. Ke, Y. W. Jung, L. F. Kourkoutis, J.-W. Kim, P. J. Ryan, T. Heeg, M. Roeckerath *et al.*, A strong ferroelectric ferromagnet created by means of spin–lattice coupling, Nature (London) **466**, 954 (2010).

[9] J. Hlinka, J. Petzelt, S. Kamba, D. Noujni, and T. Ostapchuk, Infrared dielectric response of relaxor ferroelectrics, Phase Transitions **79**, 41 (2006).

[10] See Supplemental Material at http://link.aps.org/supplemental/10.1103/PhysRevB.108.224308 for first-principles calculations details, projections of mode character as a function of strain, and phonon frequency as a function of electron doping, which includes Refs. [25–29].

[11] Y. Yang, W. Ren, D. Wang, and L. Bellaiche, Understanding and revisiting properties of $EuTiO_3$ bulk material and films from first principles, Phys. Rev. Lett. **109**, 267602 (2012).

[12] J. C. Slater, The Lorentz correction in barium titanate, Phys. Rev. **78**, 748 (1950).

[13] I. B. Bersuker, Pseudo-Jahn–Teller effect—a two-state paradigm in formation, deformation, and transformation of molecular systems and solids, Chem. Rev. **113**, 1351 (2013).

[14] P. A. Franken, A. E. Hill, C. W. Peters, and G. Weinreich, Generation of optical harmonics, Phys. Rev. Lett. **7**, 118 (1961).

[15] B. Jalan, P. Moetakef, and S. Stemmer, Molecular beam epitaxy of $SrTiO_3$ with a growth window, Appl. Phys. Lett. **95**, 032906 (2009).

[16] K. Ahadi, L. Galletti, and S. Stemmer, Evidence of a topological Hall effect in $Eu_{1-x}Sm_xTiO_3$, Appl. Phys. Lett. **111**, 172403 (2017).

[17] K. Jiang, R. Zhao, P. Zhang, Q. Deng, J. Zhang, W. Li, Z. Hu, H. Yang, and J. Chu, Strain and temperature dependent absorption spectra studies for identifying the phase structure and band gap of $EuTiO_3$ perovskite films, Phys. Chem. Chem. Phys. **17**, 31618 (2015).

[18] S. Salmani-Rezaie, K. Ahadi, W. M. Strickland, and S. Stemmer, Order-disorder ferroelectric transition of strained $SrTiO_3$, Phys. Rev. Lett. **125**, 087601 (2020).

[19] I.-K. Jeong, S. Lee, S.-Y. Jeong, C. J. Won, N. Hur, and A. Llobet, Structural evolution across the insulator-metal transition in oxygen-deficient $BaTiO_{3-\delta}$ studied using neutron total scattering and Rietveld analysis, Phys. Rev. B **84**, 064125 (2011).

[20] Y. Frenkel, N. Haham, Y. Shperber, C. Bell, Y. Xie, Z. Chen, Y. Hikita, H. Y. Hwang, E. K. H. Salje, and B. Kalisky, Imaging and tuning polarity at $SrTiO_3$ domain walls, Nat. Mater. **16**, 1203 (2017).

[21] J. Seidel, L. W. Martin, Q. He, Q. Zhan, Y.-H. Chu, A. Rother, M. E. Hawkridge, P. Maksymovych, P. Yu, M. Gajek, N. Balke, S. V. Kalinin, S. Gemming, F. Wang, G. Catalan, J. F. Scott, N. A. Spaldin, J. Orenstein, and R. Ramesh, Conduction at domain walls in oxide multiferroics, Nat. Mater. **8**, 229 (2009).

[22] M. Porer, M. Fechner, M. Kubli, M. J. Neugebauer, S. Parchenko, V. Esposito, A. Narayan, N. A. Spaldin, R. Huber, M. Radovic, E. M. Bothschafter, J. M. Glownia, T. Sato, S. Song, S. L. Johnson, and U. Staub, Ultrafast transient increase of oxygen octahedral rotations in a perovskite, Phys. Rev. Res. **1**, 012005(R) (2019).

[23] C. Paillard, E. Torun, L. Wirtz, J. Íñiguez, and L. Bellaiche, Photoinduced phase transitions in ferroelectrics, Phys. Rev. Lett. **123**, 087601 (2019).

[24] K. Ahadi, L. Galletti, Y. Li, S. Salmani-Rezaie, W. Wu, and S. Stemmer, Enhancing superconductivity in $SrTiO_3$ films with strain, Sci. Adv. **5**, eaaw0120 (2019).

[25] G. Kresse and J. Furthmüller, Efficient iterative schemes for *ab initio* total-energy calculations using a plane-wave basis set, Phys. Rev. B **54**, 11169 (1996).

[26] G. Kresse and D. Joubert, From ultrasoft pseudopotentials to the projector augmented-wave method, Phys. Rev. B **59**, 1758 (1999).

[27] J. P. Perdew, A. Ruzsinszky, G. I. Csonka, O. A. Vydrov, G. E. Scuseria, L. A. Constantin, X. Zhou, and K. Burke, Restoring the density-gradient expansion for exchange in solids and surfaces, Phys. Rev. Lett. **100**, 136406 (2008).

[28] P. E. Blöchl, Projector augmented-wave method, Phys. Rev. B **50**, 17953 (1994).

[29] A. I. Liechtenstein, V. I. Anisimov, and J. Zaanen, Density-functional theory and strong interactions: Orbital ordering in Mott-Hubbard insulators, Phys. Rev. B **52**, R5467(R) (1995).